AIP Applied Physics Letters

Bandgap engineering by tuning particle size and crystallinity of SnO2–Fe2O3 nanocrystalline composite thin films

M. B. Sahana, C. Sudakar, G. Setzler, A. Dixit, J. S. Thakur et al.

Citation: Appl. Phys. Lett. **93**, 231909 (2008); doi: 10.1063/1.3042163
View online: http://dx.doi.org/10.1063/1.3042163
View Table of Contents: http://apl.aip.org/resource/1/APPLAB/v93/i23
Published by the American Institute of Physics.

Related Articles

Studying periodic nanostructures by probing the in-sample optical far-field using coherent phonons
Appl. Phys. Lett. 101, 243117 (2012)

Negative Gaussian curvature distribution in physical and biophysical systems—Curved nanocarbons and ion-channel membrane proteins
J. Appl. Phys. 112, 114316 (2012)

Room-temperature ferromagnetism in Co-doped CeO2 nanospheres prepared by the polyvinylpyrrolidone-assisted hydrothermal method
J. Appl. Phys. 112, 113904 (2012)

Surface-enhanced Raman scattering (SERS) based on copper vanadate nanoribbon substrate: A direct bio-detection without surface functionalization
J. Appl. Phys. 112, 114309 (2012)

Modeling plasmonics: A Huygens subgridding scheme for Lorentz media
J. Chem. Phys. 137, 204111 (2012)

Additional information on Appl. Phys. Lett.

Journal Homepage: http://apl.aip.org/
Journal Information: http://apl.aip.org/about/about_the_journal
Top downloads: http://apl.aip.org/features/most_downloaded
Information for Authors: http://apl.aip.org/authors

ADVERTISEMENT

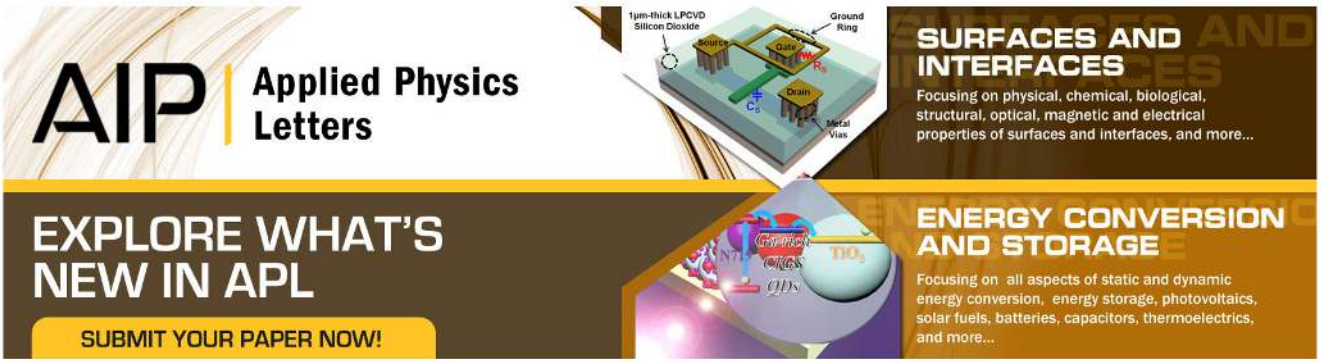

Bandgap engineering by tuning particle size and crystallinity of $SnO_2-Fe_2O_3$ nanocrystalline composite thin films

M. B. Sahana,[1] C. Sudakar,[1,a)] G. Setzler,[1] A. Dixit,[1] J. S. Thakur,[1] G. Lawes,[1] R. Naik,[1] V. M. Naik,[2] and P. P. Vaishnava[3]
[1]*Department of Physics and Astronomy, Wayne State University, Detroit, Michigan 48201, USA*
[2]*Department of Natural Sciences, University of Michigan-Dearborn, Dearborn, Michigan 48128, USA*
[3]*Department of Physics, Kettering University, Flint, Michigan 48504, USA*

(Received 23 October 2008; accepted 13 November 2008; published online 11 December 2008)

We report the structural and optical properties of $xSnO_2-yFe_2O_3$ nanocrystalline composite thin films. SnO_2 and Fe_2O_3 exhibit strong phase separation instability and their particle size and crystallinity are tunable by changing their composition and annealing temperature. The bandgap for these composites continuously increases from 2.3 to 3.89 eV. We discuss the increasing bandgap values in terms of the quantum confinement effect manifested by the decreasing size of Fe_2O_3 crystallites. The method provides a generic approach for the tuning of the bandgap in nanocomposite systems. © *2008 American Institute of Physics*. [DOI: 10.1063/1.3042163]

Understanding the interplay between the nanoscale structure and optical properties of semiconductors (SC) is essential for incorporating these systems into technological applications that require tunable energy gaps, including solar cells[1] and optoelectronic devices.[2] Thin films of nanocrystalline heterogeneous composites consisting of SC particles are promising materials for these applications as they offer considerable flexibility in tuning the properties. The material properties of nanostructured composites often differ from the individual bulk components because of strong surface interactions and the quantum confinement effects.

The bandgap is one of the fundamental properties exploited in many technological applications, and for some materials it can be tuned by alloying. A number of oxide alloys, such as MgZnO and CdZnO,[3] have been studied to understand how the alloying composition affects the optical bandgap. The phase segregation generally observed in many of these materials has a negative impact on the ability to controllably tune the bandgap by alloying. Recently Khoshman *et al.*[4] obtained bandgap tunability in Be_xZn_yO nanocomposite over a large energy range by minimizing the lattice mismatch effects in their amorphous alloy phases. Alternatively, in nanocrystallites the desired values of the bandgap[5] can be modified by quantum confinement effects by varying the size of these nanocrystallites. Though several studies reported on the bandgap tunability of particles by decreasing their size, investigations on composite nanocrystalline materials are sparse.

Materials with tunable bandgap are appropriate for photovoltaic and photocatalytic applications. α-Fe_2O_3, an *n*-type SC with a bandgap E_g of 2.2 eV, is promising as a photoelectrode for efficient conversion of solar energy[6] and also as gas sensors and catalysts.[7,8] Likewise SnO_2 is a *n*-type wide bandgap SC with a E_g of 3.7 eV and has been a widely studied oxide material for a number of applications including optoelectronic devices, gas sensors, photocatalysts, and electrodes.[9] However, the composite oxide α-$Fe_2O_3-SnO_2$ system, which has a high sensitivity to CH_4 and C_2H_5OH (Ref. 10) and potential for bandgap tunability, has not been studied in detail for optical and electronic applications.

In this paper we report the fabrication of heterogeneous nanocomposites thin films of $SnO_2-Fe_2O_3$ starting from a homogeneously mixed precursor solution. We found that SnO_2 and Fe_2O_3 phases are completely immiscible. The particle size of the SnO_2 and Fe_2O_3 phases can be controlled by tuning the composition and postdeposition annealing conditions. Our studies establish that the bandgap in these composite materials can be tuned from the SnO_2 bandgap (3.89 eV) to the Fe_2O_3 bandgap (2.3 eV) by modifying the particle size and crystallinity of the Fe_2O_3 phase. We find that the observed particle size dependent bandgap tunability is related to quantum confinement effects.

$xSnO_2-yFe_2O_3$ thin films (0.5–1 μm) having a range of compositions ($x=0-1$, $y=(1-x)/2$) were prepared by spin coating of metal-organic precursors.[11] The thin films were deposited on single crystal sapphire (006) substrates and annealed in air at 600 °C. The crystal structure and composition of these films were determined using x-ray diffraction (XRD). The XRD patterns of pure SnO_2 show broad reflections consistent with crystalline nanoparticles [Fig. 1(a)]. For $xSnO_2-yFe_2O_3$ thin films with $x=0.8$ to 0.6, the XRD patterns show only peaks consistent with the SnO_2 phase with no indication of any secondary Fe_2O_3 structure or any impurity phases. However, the SnO_2 reflections broaden with increasing Fe concentration and at $x=0.4$ the film is completely x-ray amorphous. With further increase in Fe in $xSnO_2-yFe_2O_3$ ($x=0.2$) the XRD shows only Fe_2O_3 peaks with no SnO_2 reflections. Pure Fe_2O_3 thin films were highly oriented along the *c*-axis. The particle size of the SnO_2 estimated using the Scherrer equation is ~10 nm for pure SnO_2 and decreases to ~2 nm for the $x=0.4$ sample. Pure Fe_2O_3 and the $xSnO_2-yFe_2O_3$ ($x=0.2$) film show iron oxide particle sizes of ≥30 nm. From these XRD studies we find that the particle size is strongly influenced by the ratio of Sn and Fe in the composite but find no evidence for any crystalline secondary phases other than SnO_2 and Fe_2O_3.

In order to more carefully examine the composition of these samples, we recorded Raman spectra of the $xSnO_2-yFe_2O_3$ samples to analyze the phase content [Fig. 1(b)]. Pure SnO_2 shows broad A_{1g} peak at 634 cm^{-1} and a

a)Author to whom correspondence should be addressed. Electronic mail: csudakar@gmail.com.

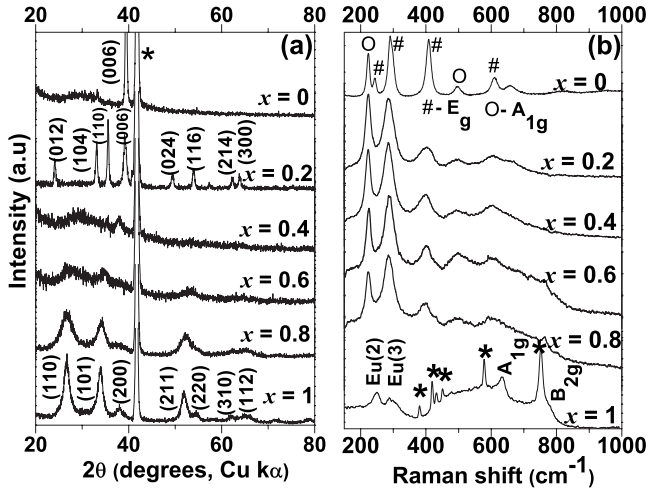

FIG. 1. (a) XRD of $x\mathrm{SnO_2}-y\mathrm{Fe_2O_3}$ (x=0 to 1) thin films. The (hkl) reflections for x=1 correspond to pure $\mathrm{SnO_2}$. $\mathrm{Fe_2O_3}$ (hkl) reflections are shown for x=0.2 and 0. (b) Raman spectra of $x\mathrm{SnO_2}-y\mathrm{Fe_2O_3}$ (x=0 to 1) thin films. The Raman modes for $\mathrm{SnO_2}$ and $\mathrm{Fe_2O_3}$ are shown for x=1 and x=0 respectively. * marked peaks are due to sapphire substrate.

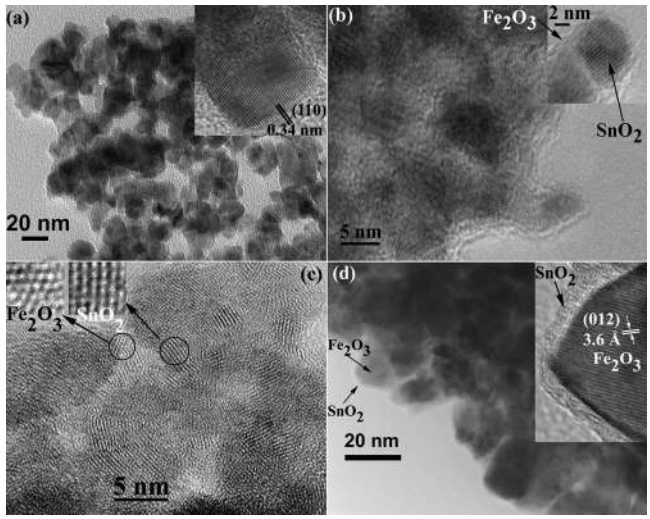

FIG. 2. TEM images of $x\mathrm{SnO_2}-y\mathrm{Fe_2O_3}$ for (a) x=1, (b) x=0.6, (c) x=0.4, and (d) x=0.2. Insets: HRTEM images of (a) one $\mathrm{SnO_2}$ crystallite. (b) (100) oriented $\mathrm{SnO_2}$ nanoparticle coated with $\mathrm{Fe_2O_3}$. (c) (−123) and (100) oriented $\mathrm{Fe_2O_3}$ and $\mathrm{SnO_2}$ nanocrystallites, respectively, are shown from regions marked with circle. (d) $\mathrm{Fe_2O_3}$ crystallite with poor crystalline $\mathrm{SnO_2}$ coating is shown.

weak B_{2g} peak at 773 $\mathrm{cm^{-1}}$.[12] The spectra also exhibit a broadband around 550 $\mathrm{cm^{-1}}$ related to some oxygen deficient disordered surface modes.[12] There are also clear bands at 250 and 300 $\mathrm{cm^{-1}}$, which are attributed to surface defect modes. The Raman signal from $\mathrm{SnO_2}$ is weak compared to the $\mathrm{Fe_2O_3}$ phase. Therefore, even a small amount of $\mathrm{Fe_2O_3}$ in the $x\mathrm{SnO_2}-y\mathrm{Fe_2O_3}$ films can be easily detected from the Raman spectra. For all samples containing Fe (x=0.8 to 0), we observe that the expected phonon modes of $\mathrm{Fe_2O_3}$ have good agreement with previous studies,[13] with no additional new modes observed. The A_{1g} modes at 224 and 496 $\mathrm{cm^{-1}}$ and E_g modes at 243, 293, 298, 413, and 609 $\mathrm{cm^{-1}}$ are marked in Fig. 1(b). We conclude that hematite is present as a secondary phase in all samples containing Fe.

The microstructure of samples annealed at 600 °C was examined by transmission electron microscopy (TEM) and high-resolution TEM (HRTEM) to determine the particle size and distribution of the $\mathrm{SnO_2}$ and $\mathrm{Fe_2O_3}$ phases. Typical HRTEM micrographs for $x\mathrm{SnO_2}-y\mathrm{Fe_2O_3}$ with x=1, 0.6, 0.4, and 0.2 are shown in Fig. 2. Pure $\mathrm{SnO_2}$ (x=0) has an average particle size around 10–15 nm, consistent with the estimate from the XRD data. The $x\mathrm{SnO_2}-y\mathrm{Fe_2O_3}$ (x=0.8 to 0) films clearly exhibit a composite microstructure. At x=0.6 we observe that the $\mathrm{SnO_2}$ particles have a size of around 3–5 nm and that these particles are uniformly coated with an amorphous phase of $\mathrm{Fe_2O_3}$ [Fig. 2(b) and inset]. At intermediate Fe concentrations, x=0.4, both the $\mathrm{SnO_2}$ and $\mathrm{Fe_2O_3}$ phases have particle sizes of only 1–2 nm and appear to be highly disordered. Typical regions consisting of a mixture of $\mathrm{SnO_2}$ and $\mathrm{Fe_2O_3}$ structures are marked in Fig. 2(c), and the HRTEM images from typical regions showing the unique symmetry of $\mathrm{SnO_2}$ and $\mathrm{Fe_2O_3}$ are shown in the inset of Fig. 2(c). For higher Fe concentrations, $\mathrm{Fe_2O_3}$ crystallites of ~20–30 nm are formed with the $\mathrm{SnO_2}$ phase present in a crystalline or amorphous form on the surface of these $\mathrm{Fe_2O_3}$ nanoparticles [Fig. 2(d)]. The energy dispersive x-ray spectroscopy analysis on the crystal shown in Fig. 3(d) shows $\mathrm{SnO_2}$ rich surface and the interior is completely comprised of $\mathrm{Fe_2O_3}$ (not shown). This analysis suggests that the largest nanoparticles are present in pure films, with increasing heterogeneity leading to a reduction in their characteristic size.

The TEM studies confirm that the films consist of an immiscible composition of the two phases at the nanoscale.

We studied the optical properties of these composite films to investigate how the nanostructure affects the optical characteristics of these SC composites. Transmittance spectra of $x\mathrm{SnO_2}-y\mathrm{Fe_2O_3}$ films were measured at room temperature using an ultraviolet-visible spectrometer. We find that the absorption edge is redshifted with increasing $\mathrm{Fe_2O_3}$ content in $\mathrm{SnO_2}$ (supplementary Fig. A).[14] In order to estimate the bandgap (E_g), we fit a straight line to the α^2 versus energy curve, assuming $\alpha^2 \propto (h\nu - E_g)$, where α is the absorption coefficient and $h\nu$ is the photon energy [Fig. 3(a)]. The bandgap decreases rapidly from 3.89 to 3.11 eV with the initial increase in Fe concentration to 20%, and it continues to decrease more slowly as the Fe content is increased. These optical measurements show that the bandgap of nanostructured films can be controllably varied from 3.89 to 2.2 eV by changing the Fe concentration in $\mathrm{SnO_2}$. We note that the transmission spectrum exhibits only one absorption edge with no discernible shoulder on the lower energy side, indicating an absence of any secondary phase related absorption edges. These results suggest that modifying the nanostructure of composite materials may provide a promising method for

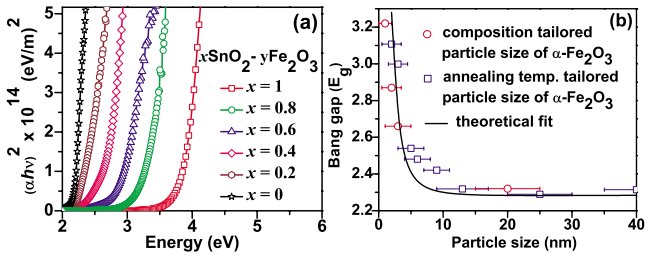

FIG. 3. (Color online) (a) $(\alpha h\nu)^2$ vs energy plots. (b) The bandgap (E_g) vs particle size of $\mathrm{Fe_2O_3}$ tailored by changing the composition of $x\mathrm{SnO_2}-y\mathrm{Fe_2O_3}$ (red circles) and by annealing $0.6\mathrm{SnO_2}-0.4\mathrm{Fe_2O_3}$ sample from 600 to 950 °C (blue squares). The theoretical fit for the bandgap change due to confinement effect in $\mathrm{Fe_2O_3}$ (see text for details). The error bars for the particle size represents the distribution in the size of the $\mathrm{Fe_2O_3}$ particles.

bandgap engineering over a wide range of energies. From XRD and TEM studies we observed that the particle size depends on the composition; therefore, we have studied the effect of particle size varied by annealing temperature on the bandgap in one of the composite films.

It is known that quantum confinement effects in SC nanoparticles increase the bandgap energy relative to bulk materials. In order to probe the effects of the crystallite sizes of the SnO_2 and Fe_2O_3 phases in tuning the bandgap, we conducted structural and optical studies on one particular sample treated at different annealing temperatures. We considered $x=0.6$ ($0.6SnO_2-0.2Fe_2O_3$) sample, which, when annealed at 600 °C, has homogeneously distributed SnO_2 and Fe_2O_3, nanoparticles with sizes in the range of 2–5 nm and a bandgap ~3 eV. We determined the particle size and crystal structure for samples annealed at different temperatures using XRD (supplementary Fig. B).[14] We collected HRTEM images to analyze the particle size and crystallinity and study the changes in morphology; representative images are shown in the inset of supplementary Fig. B.[14]

We find clear evidence for a systematic increase in SnO_2 particle size as the annealing temperature is increased from 600 to 950 °C, as observed in the broad (110) and (101) reflections evolving into narrow peaks at 950 °C. The particle size of SnO_2 increases from 2–5 nm for the 600 °C annealed sample to >30 nm for sample annealed at 950 °C. In addition, at temperature above 700 °C we see the onset of Fe_2O_3 diffraction peaks, which are fully evolved in the 950 °C annealed samples. The temperature dependent increase in the size of the SnO_2/Fe_2O_3 particles in the presence of Fe_2O_3/SnO_2 can be understood by the increased diffusion parameters during thermal treatments.[15] These measurements show evidence for phase segregation of SnO_2 and Fe_2O_3 and increasing particle size and crystallinity in the Fe_2O_3 component as the annealing temperature is increased. The optical transmission spectra of $xSnO_2-yFe_2O_3$ ($x=0.6$) films annealed at 600 °C yield $E_g=3.1$ eV, with the bandgap decreasing with increasing annealing temperature, as shown in the supplementary Fig. B.[14] The bandgap of the 950 °C annealed sample is about 2.3 eV. The inset in supplementary Fig. B[14] shows the change in the bandgap of $0.6SnO_2-0.2Fe_2O_3$ at different annealing temperatures.

Figure 3(b) clearly shows that the bandgap of the composite increases as the Fe_2O_3 particle size decreases. The largest bandgap energy measured in these samples is smaller than the bandgap of SnO_2 suggesting that absorption is always dominated by the Fe_2O_3 nanocrystallite phase, and the SnO_2 phase has a minimal effect on the optical absorption. Motivated by this experimental result, we discuss the correlation between the bandgap values and the sizes of nanocrystallite Fe_2O_3 phase in the context of quantum confinement. These finite size effects are normally investigated in isolated nanoparticles, where the size can be varied to tune the bandgap. Our samples consist of immiscible phases of Fe_2O_3 and SnO_2 in nanocomposite thin films and can be simply modeled as a large and small bandgap nanocomposite. If the lower bandgap nanocrystallite phase has a small physical size, the bandgap will increase due to the additional energy from the degree of confinement and Coulomb correlations, so the effective bandgap becomes[16]

$$E_g = E_g^o + \frac{n^2\hbar^2\pi^2}{2\mu R^2} - \frac{1.8e^2}{\varepsilon R}, \quad (1)$$

where E_g^o is the bandgap of the bulk Fe_2O_3 and R is the size of the nanocrystallites. In this expression, e is the electron charge, ε is the effective dielectric constant, and μ is the reduced effective mass of electron and hole of Fe_2O_3. In the above equation, we used $\varepsilon=5.7$, $\mu=0.08m_0$ (m_0 is the electron's rest mass). For E_g^o we took the lowest value we measured in our experiments. The good agreement between the theoretical fit and the data, as shown in Fig. 3(b), demonstrates that the optical response of the nanocomposite is dominated by quantum confinement effects in the Fe_2O_3 crystallites. These confinement effects begin to influence the optical properties of Fe_2O_3 crystallites when their size becomes smaller than 6.0 nm, with the largest blueshift of about 1.0 eV produced by the 2 nm sizes crystallites.

In this study we show that $xSnO_2-yFe_2O_3$ ($1 \leq x \leq 0$) material does not form a stable alloy but exhibits strong phase separation instability in favor of SnO_2 and Fe_2O_3 phases. The size of these phases depends on the composition and can also be controlled by annealing temperatures. The bandgap measured from the optical properties of the composites show variations in the values, which are found to be related to the size of the Fe_2O_3 nanaocrystallites. We discuss this correlation between the bandgap values and the nanaocrystallites size in terms of the quantum confinement effect due to the size of Fe_2O_3 nanaocrystallites. This study demonstrates that the bandgap value of the Fe_2O_3 can be engineered by decreasing the size of the Fe_2O_3 nanoparticle in a nanocomposite system. The bandgap tunability and strong optical absorption with high chemical stability make this material a potential candidate for many nanotechnology based applications.

This research was supported by the National Science Foundation under NSF CAREER Grant No. DMR-06044823 and by the Institute for Manufacturing Research at Wayne State University.

[1] S. Ferrere, A. Zaban, and B. A. Gregg, J. Phys. Chem. B **101**, 4490 (1997).
[2] T. Hayakawa and M. Nogami, Sci. Technol. Adv. Mater. **6**, 66 (2005).
[3] T. Makino, Y. Segawa, M. Kawasaki, A. Ohtomo, R. Shiroki, K. Tamura, and T. Yasuda, Appl. Phys. Lett. **78**, 1237 (2001).
[4] J. M. Khoshman, D. C. Ingram, and M. E. Kordesch, Appl. Phys. Lett. **92**, 091902 (2008).
[5] M. Li and J. C. Li, Mater. Lett. **60**, 2526 (2006).
[6] Y. Wang, T. Yu, X. Chen, H. Zhang, S. Ouyang, Z. Li, J. Ye, and Z. Zou, J. Phys. D **40**, 3925 (2007).
[7] H. H. Kung, *Transition Metal Oxides: Surface Chemistry and Catalysis* (Elsevier, New York, 1989).
[8] L. Huo, W. Li, L. Lu, H. Cai, S. Xi, J. Wang, B. Zhao, Y. Shen, and Z. Lu, Chem. Mater. **12**, 790 (2000).
[9] M. Batzill and U. Diebold, Prog. Surf. Sci. **79**, 47 (2005).
[10] M. Takano, Y. Bando, N. Nakanishi, M. Sakai, and H. Okinaka, J. Solid State Chem. **68**, 153 (1987).
[11] C. Sudakar, P. Kharel, G. Lawes, R. Suryanarayanan, R. Naik, and V. M. Naik, J. Phys.: Condens. Matter **19**, 026212 (2007).
[12] J. X. Zhou, M. S. Zhang, J. M. Hong, J. L. Fang, and Z. Yin, Appl. Phys. A: Mater. Sci. Process. **81**, 177 (2005).
[13] S.-H. Shim and T. S. Duffy, Am. Mineral. **87**, 318 (2002).
[14] See EPAPS Document No. E-APPLAB-93-061849 for transmission spectra of 600 °C annealed composites and XRD, HRTEM and transmission spectra of $x=0.6$ annealed at 600 to 950 °C for the black square box. For more information on EPAPS, see http://www.aip.org/pubservs/epaps.html.
[15] R. H. R. Castro, R. Pilar Hidalgo Muccillo, and D. Gouvea, Appl. Surf. Sci. **214**, 172 (2003).
[16] L. Brus, J. Phys. Chem. **90**, 2555 (1986).